

RESEARCH ARTICLE

10.1002/2014JC010189

Key Points:

- Time series analysis on Bio-Argo float data
- The seasonal dynamics of bio-optical properties
- The intercorrelation between bio-optical properties

Correspondence to:

X. Xing,
xing@ouc.edu.cn

Citation:

Xing, X., H. Claustre, J. Uitz, A. Mignot, A. Poteau, and H. Wang (2014), Seasonal variations of bio-optical properties and their interrelationships observed by Bio-Argo floats in the subpolar North Atlantic, *J. Geophys. Res. Oceans*, 119, doi:10.1002/2014JC010189.

Received 27 MAY 2014

Accepted 6 OCT 2014

Accepted article online 8 OCT 2014

Seasonal variations of bio-optical properties and their interrelationships observed by Bio-Argo floats in the subpolar North Atlantic

Xiaogang Xing^{1,2}, Hervé Claustre^{3,4}, Julia Uitz^{3,4}, Alexandre Mignot⁵, Antoine Poteau^{3,4}, and Haili Wang²

¹Key Laboratory of Physical Oceanography, Ministry of Education, Ocean University of China, Qingdao, China, ²State Key Laboratory of Marine Environmental Science, Xiamen University, Xiamen, China, ³Sorbonne Universités, UMR 7093, UPMC Université Paris 6, LOV, Observatoire Océanologique de Villefranche, Villefranche-sur-Mer, France, ⁴CNRS, UMR 7093, LOV, Observatoire Océanologique de Villefranche, Villefranche-sur-Mer, France, ⁵Department of Earth, Atmospheric and Planetary Sciences, Massachusetts Institute of Technology, Cambridge, Massachusetts, USA

Abstract Based on in situ data sets collected using two Bio-Argo floats deployed in the subpolar North Atlantic from June 2008 to May 2010, the present study focuses on the seasonal variability of three bio-optical properties, i.e., chlorophyll-a concentration ([Chla]), particle backscattering coefficient at 532 nm ($b_{bp}(532)$), and particle beam attenuation coefficient at 660 nm ($c_p(660)$). In addition, the interrelationships among these properties are examined. Our results show that: (1) [Chla], $b_{bp}(532)$ and $c_p(660)$ are largely well coupled with each other in the upper layer, all being minimum in mid-winter (January) and maximum in summer; (2) the backscattering coefficient presents an abrupt increase in late summer in the Icelandic Basin, likely due to a large contribution of coccolithophores following the diatom spring bloom; (3) the intercorrelations between the three bio-optical properties are basically consistent with previous studies; (4) seasonal variation in the of [Chla] to $c_p(660)$ ratio exhibits a clear light-dependence, most likely due to the phytoplankton photoacclimation.

1. Introduction

Since the term “bio-optics” was introduced in the late 1970s [Smith and Baker, 1978], several bio-optical studies have focused on the variability and relationships between the concentrations of optically significant biogeochemical constituents (e.g., chlorophyll-a, particulate and dissolved organic carbon) and the so-called inherent optical properties (IOPs). On the basis of these studies and established relationships, the observation of bio-optical properties could in turn be used to assess the variability of biological and biogeochemical states at diverse spatial and temporal scales [Gordon and Morel, 1983; Morel and Bricaud, 1986; Loisel and Morel, 1998; Bricaud et al., 1998; Morel and Maritorena, 2001; Huot et al., 2008; Claustre et al., 2008; Loisel et al., 2011; Antoine et al., 2011]. For instance, chlorophyll fluorescence provides a proxy for chlorophyll-a concentrations ([Chla]) [Lorenzen, 1966; Holm-Hansen et al., 2000; Loisel et al., 2011], while the particle beam attenuation (c_p) at 660 nm is usually correlated, in open ocean waters, with the concentration of particulate organic carbon (POC) [Gardner et al., 1985; Bishop, 1986; Bishop et al., 1999; Claustre et al., 1999; Cetinić et al., 2012]. Moreover, the particle backscattering coefficient (b_{bp}) is also used to infer the POC abundance and phytoplankton biomass [Stramski et al., 1999; Balch et al., 2001; Boss and Behrenfeld, 2010], although it is often considered, as a result of theoretical studies based on the Mie theory [Morel and Ahn, 1991; Stramski and Kiefer, 1991], to be more sensitive to the contribution of small particles than the total (forward + backward) scattering (as well as beam attenuation).

Over the last decade, multiple bio-optical relationships have been established based on global data sets, some of them being the basis for the retrieval of biogeochemical properties from a satellite platform [e.g., O'Reilly et al., 1998; Morel et al., 2007]. However, ocean color radiometry has its intrinsic limitations. First, it cannot provide information on the vertical distribution of bio-optical variables, and so needs to be supplemented by extensive acquisitions of in situ profiles along the water column. Second, its capability is limited by low sunlight intensity and cloud coverage, especially in certain high latitudinal oceanic regions (e.g., the subpolar Atlantic, Arctic, and Southern Ocean). As a consequence, satellites cannot provide frequent observations over the winter period and data gaps can last for several months. It is still necessary, therefore, to

reinforce satellite observations with in situ observations in these regions in order to improve our knowledge of the seasonal cycles and vertical distributions of bio-optical and hence biogeochemical properties.

In situ observations based on conventional ship-based platforms are scarce. Generally, ship-based observations cover a large range of spatial scales; however they often under-sample the temporal variability in a given basin [e.g. *Claustre et al.*, 2008]. Indeed, for obvious cost-effectiveness reasons, time-series observations are restricted to oceanic regions easily accessible from ships, leaving rather undocumented most remote open ocean waters. This limitation in our present observation capabilities severely constrains our understanding of the optical variability and related biogeochemical processes at the seasonal scale.

Recently, the development of a profiling float dedicated to bio-optical observations and especially the subsequent development of an associated network has been recommended by the international community [*Claustre et al.*, 2010; *International Ocean-Color Coordinating Group (IOCCG)*, 2011]. The so-called Bio-Argo float, consists of traditional Argo T/S float equipped with bio-optical sensors, thus allowing long-term measurements of certain bio-optical variables (e.g., chlorophyll-a fluorescence, CDOM fluorescence, backscattering coefficient, beam attenuation coefficient, radiometry, etc.) to be conducted autonomously with a high vertical (~ 1 m) and temporal (less than 10 days) resolution at basin scale [*Boss et al.*, 2008; *Bishop and Wood*, 2009; *Claustre et al.*, 2010; *Xing et al.*, 2014; *Mignot et al.*, 2014].

The onset of phytoplankton blooms and their fate in the North Atlantic represent an important matter of debate [e.g., *Behrenfeld*, 2010; *Strutton et al.*, 2011; *Taylor and Ferrari*, 2011; *Behrenfeld et al.*, 2013; *Behrenfeld and Boss*, 2014]. Nevertheless, the scarcity of in situ data related to the cycles of biological and biogeochemical properties at these latitudes represents a significant limitation for a proper understanding of the mechanisms at play. Thanks to the availability of autonomous platforms, first in situ long-term chlorophyll and backscattering time series were obtained with a Bio-Argo float [*Boss et al.*, 2008] and used to better characterize the bloom dynamics in the western North Atlantic [*Boss and Behrenfeld*, 2010]. The beam attenuation coefficient was, however, not recorded in these studies. Furthermore, the vertical distribution and interrelationships between chlorophyll and backscattering were not analyzed in detail.

In summer 2008, two Bio-Argo floats equipped with multiple sensors (including in particular, a chlorophyll fluorometer, a backscattering sensor and a transmissometer) were deployed in the subpolar North Atlantic. This was the first time that several bio-optical properties could be measured simultaneously over the vertical and over full seasonal cycles. In the almost 2 year period, these two floats recorded more than 160 bio-optical and hydrological profiles. Based on these data, the present study aims at characterizing the vertical and seasonal distributions of these bio-optical properties and to analyze their interrelationships. The objective of this analysis is to develop a better understanding of the coupling/decoupling between different bio-optical properties, as well as their dependence on hydrographic conditions. In addition, because most previously published bio-optical relationships have been established through measurements acquired during summer-autumn cruises, there might probably be bias. It is therefore of interest to reconsider these relationships in light of the present data that are temporally unbiased.

2. Materials and Methods

2.1. Float Data

In the summer of 2008, two Bio-Argo floats were deployed in the subpolar North Atlantic for long-term bio-optical and hydrological observations. Their trajectories and observation location are shown in Figure 1. One float was deployed in the Iceland Basin (numbered as "B03") and the other one in the Irminger Sea (numbered as "B01"). The B03 float remained in the Iceland Basin for about 1 year from May 2009, and then drifted toward the northeast. In the beginning of August 2009, it passed through the Iceland-Faroe Ridge into the Norwegian Sea. Until May 2010 (battery depleted), this float had recorded 123 hydrological and bio-optical profiles. The B01 float always stayed in the Irminger Sea and collected 42 profiles over a nearly 10 month lifetime.

Both floats were designed to profile once every 2–10 days. Physical parameters were recorded from 1000 m to the surface, while bio-optical properties were only measured from 400 m up to the surface. However, just before each profile, all the bio-optical sensors were programmed to acquire data for 5 min at the parking depth (1000 m), providing a useful reference for examining the potential drift of the sensors.

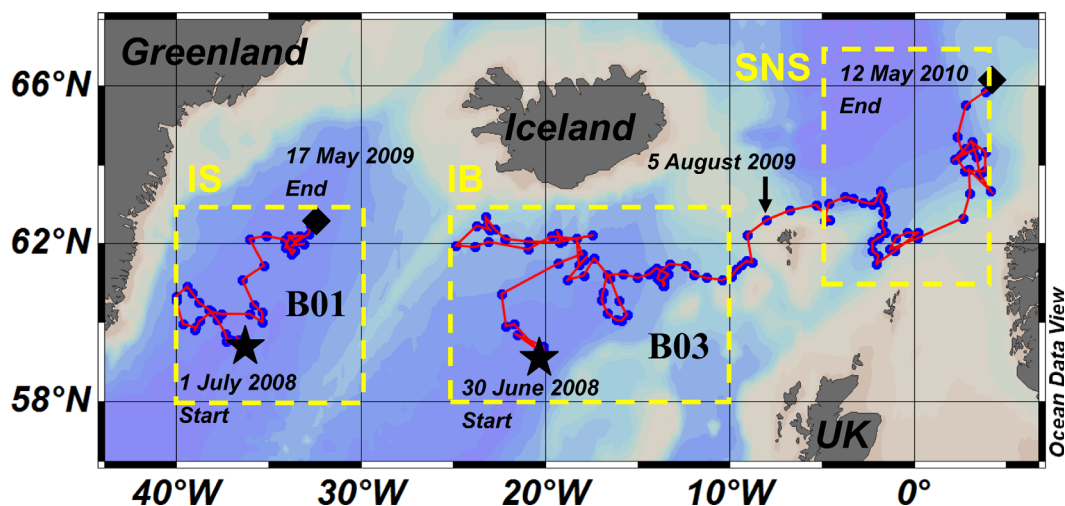


Figure 1. Trajectories and observation positions of the two Bio-Argo floats (numbered as “B03” and “B01”) deployed in the subpolar North Atlantic. The stars represent the first profiles, and the diamonds the last ones.

The [Chla] (mg m^{-3}) was retrieved using a combined processing [Xing *et al.*, 2011] based on the downward irradiance at 490 nm (Satlantic radiometer) and chlorophyll fluorescence (Wetlabs fluorometer, Ex/Em at 470/695 nm). The [Chla] retrieval equation can be written as:

$$[\text{Chla}] = F_{490}(\text{Fluo} - \text{Offset}) \quad (1)$$

where Fluo represents the in situ measured chlorophyll fluorescence after factory calibration, [Chla] is the retrieved chlorophyll-a concentration, Offset represents the instrumental dark signal (it should be zero if the fluorometer is well calibrated by the manufacturer) and F_{490} a conversion coefficient.

The instrumental dark signal of each fluorometer was examined through the measurements at the parking depth (i.e., ~ 1000 m). As shown in Figure 2a, the deep chlorophyll fluorescence values were quite stable for each float, reaching 0.1331 ± 0.007 and 0.026 ± 0.011 for B03 and B01, respectively. Since the chlorophyll-a concentration is commonly assumed to be zero at such depths, the nonzero but stable fluorescence value at 1000 m was considered as biased factory calibration and thus subtracted from all profiles (i.e., the Offset in equation (1)). Following this correction step, a quenching correction procedure, introduced by Xing *et al.* [2012], was used to remove the influence of nonphotochemical quenching on the fluorescence signal at surface. Finally, F_{490} was determined through the method of Xing *et al.* [2011], that makes simultaneous use of the chlorophyll-a fluorescence profiles, of the diffuse attenuation coefficient, $K_d(490)$, and of an empirical relationship linking [Chla] and $K_d(490)$. The F_{490} median of all the profiles from each float (0.515 and 0.474 for B03 and B01 float, respectively) is used to finally convert all the fluorescence profiles into [Chla].

The backscattering sensor was used to measure the volume scattering coefficient at 532 nm and 117° ($\beta(117^\circ, 532)$, units $\text{m}^{-1} \text{sr}^{-1}$), which could be converted into $b_{\text{bp}}(532)$ (units m^{-1}) based on the methodology described in Boss and Pegau [2001]. In particular, the backscattering data were also offset-corrected based on the values measured at the parking depth. Although the backscattering coefficient should be positive at depth because of the presence of nonalgal particles (NAP) [Boss *et al.*, 2008], the time series of $b_{\text{bp}}(532)$ recorded at 1000 m showed obvious discrepancies between floats B01 and B03, most likely due to poor sensor calibration (Figure 2b). The values collected at the parking depth by float B01 were about 0.00038 m^{-1} , while those from float B03 were always larger than 0.00059 m^{-1} . In addition, the minimum values observed at 1000 m by float B01 (0.00031 m^{-1}) are much larger than the “expected” NAP backscattering. In the same region and over a 2 year period, Boss *et al.* [2008] inferred $b_{\text{bp}}(440)$ values of $0.00015 \text{ m}^{-1} (\pm 0.0003)$ at 1000 m. Therefore, a systematical offset correction was applied to each b_{bp} profile. The offset value used was the minimum value recorded at the parking depth for each float, i.e., 0.00059 m^{-1} for float B03 and 0.00031 m^{-1} for float B01. Then, we estimated the contribution of NAP to the b_{bp} signal at 532 nm was estimated and added the resulting value

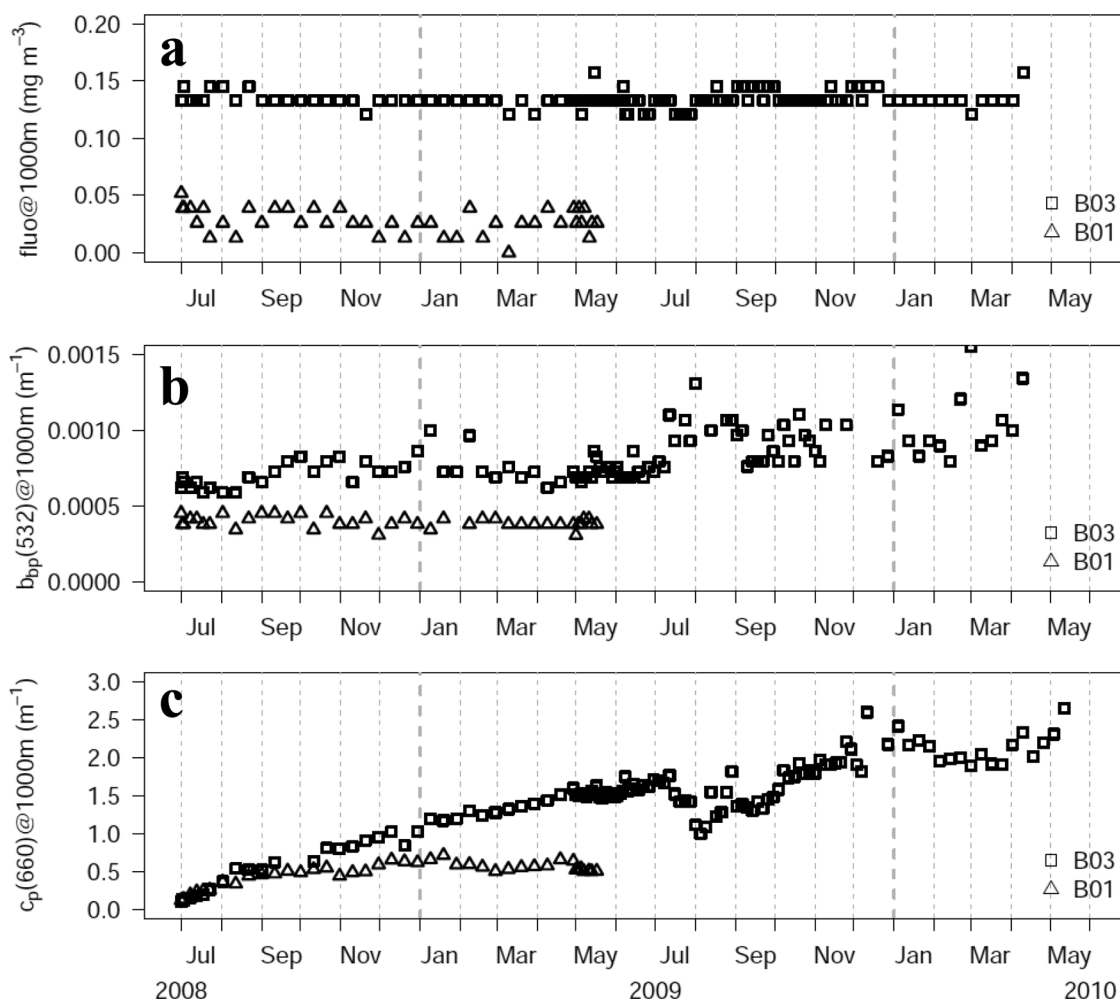


Figure 2. (a) Time series of chlorophyll-a fluorescence, (b) $b_{bp}(532)$, and (c) $c_p(660)$ at the parking depth (1000 m). The squares and triangles represent the values recorded by the B03 and B01 floats, respectively.

(0.000124 m^{-1}) was added to all $b_{bp}(532)$ profiles. This estimation is based on two assumptions: (1) the contribution of NAP to backscattering at 440 nm is 0.00015 m^{-1} in the Iceland Basin and Irminger Sea [Boss *et al.*, 2008]; (2) and the backscattering coefficient decreases exponentially with wavelength, following a spectral dependency of λ^{-1} .

The transmissometer was used to measure the beam attenuation coefficient at 660 nm [$c(660)$, units m^{-1}]. The particulate component of $c(660)$, $c_p(660)$, which can be used as a proxy of POC, was acquired via offset-correction processing, removing the bias due to particles settled on the sensor. The offset was determined as the value at parking depth on a profile-by-profile basis (Figure 2c) [Loisel and Morel, 1998]. Similarly to $b_{bp}(532)$, the contribution of NAP to $c_p(660)$ was estimated. A value of 0.01 m^{-1} was added to all $c_p(660)$ profiles based on a $b_{bp}(440)$ for NAP of 0.00015 m^{-1} [Boss *et al.*, 2008] and assuming a b_{bp}/c_p ratio of 0.01 in the North Atlantic [Westberry *et al.*, 2010].

2.2. Satellite Data

The satellite remotely sensed data (Level 3, 8 day composite, $9 \text{ km} \times 9 \text{ km}$ resolution), provided by the National Aeronautics and Space Administration (NASA) (<http://oceancolor.gsfc.nasa.gov/cgi/l3>), were used to compare with in situ float measurements and assess the sampling representativeness of the floats. These satellite data include MODIS-A [Chla] and $b_{bp}(443)$ derived from a GSM semianalytical ocean color model [Maritorena *et al.*, 2002], the daytime sea surface temperature (SST) retrieved through thermal infrared radiometry at $11 \mu\text{m}$, the particulate inorganic carbon (PIC) concentration based on a two-band look-up table approach [Balch *et al.*, 2005], and the

derived surface daily photosynthetically active radiation (PAR, units moles photons $m^{-2} d^{-1}$) using the radiative transfer model of *Frouin and Chertock* [1992] and the atmospheric properties inferred from MODIS.

For comparison between in situ particle backscattering coefficients measured by floats and MODIS retrieved ones, the GSM $b_{bp}(443)$ products were converted into their 532 nm counterparts, based on the assumption of the of λ^{-1} spectral dependency of particulate backscattering, i.e., $GSM\ b_{bp}(532) = 0.83\ GSM\ b_{bp}(443)$.

In order to match with the data recorded by the floats, the satellite data were averaged over a $0.2^\circ \times 0.2^\circ$ box centered on the position of each profile and hereafter referred to as “along-track” values. Furthermore, and with the objective to assess the representativeness of float sampling within a given region, averaged values were calculated over three main regions (Figure 1), i.e., the Iceland Basin (abbreviated as “IB,” $25^\circ W-10^\circ W, 58^\circ N-63^\circ N$), the South Norwegian Sea (abbreviated as “SNS,” $5^\circ W-4^\circ E, 61^\circ N-67^\circ N$), and the Irminger Sea (abbreviated as “IS,” $40^\circ W-30^\circ W, 58^\circ N-63^\circ N$).

2.3. Derived Data

Two kinds of mixed layer depth (MLD) values were determined based on the density and temperature profiles, respectively. The selected criteria followed *De Boyer-Montegut et al.* [2004], with MLD being the depth at which densities deviate from their 10 m value by a given threshold ($\Delta\sigma = 0.03\ kg\ m^{-3}$).

The profile of the diffuse attenuation coefficient for the whole visible light, $K_d(PAR)$, was estimated from the retrieved [Chla], based on empirical relationships [*Morel et al.*, 2007] as follows:

$$K_d(490) = 0.0166 + 0.0825[Chla]^{0.6529} \tag{2}$$

$$K_d(PAR) = 0.00665 + 0.874\ K_d(490) - 0.00121\ K_d(490)^{-1} \tag{3}$$

The penetration depth (z_{pd}) and the euphotic depth (z_{eu}) were determined according to their respective definitions:

$$\int_0^{z_{pd}} K_d(PAR, z) dz = 1 \tag{4}$$

$$\int_0^{z_{eu}} K_d(PAR, z) dz = 4.6 \tag{5}$$

The growth irradiance (I_g , units moles photons $m^{-2} h^{-1}$), defined as the median light level within the mixed layer [*Behrenfeld et al.*, 2005], was derived from the estimated $K_d(PAR)$ profile, remotely sensed surface PAR, mixed layer depth ($MLD_{d0.03}$) and local sunshine duration (in units of hour). The PAR profile was estimated following equation (6). Then the median PAR value within the mixed layer depth was calculated and divided by the sunshine duration to obtain the growth irradiance

$$PAR(z_2) = PAR(z_1) \exp[-K_d(PAR, z_1)(z_2 - z_1)] \tag{6}$$

3. Results and Discussions

3.1. Sampling Representativeness of Floats

In this section, the sampling representativeness of the two floats is examined using the MODIS remotely sensed SST, [Chla], and b_{bp} . As mentioned in section 2.2, three region-averaged values were calculated during the operating period of the floats in the Iceland Basin (IB), South Norwegian Sea (SNS), and Irminger Sea (IS).

Being drifting profiling platforms, Bio-Argo floats are neither Eulerian nor Lagrangian. Therefore, the representativeness of float sampling for the whole basin needs to be assessed before a seasonal analysis can be carried out. Indeed seasonal analysis in general assumes that the along-track sampling is typical and representative of the entire region.

Figures 3a, 3c, and 3e show a comparison of the satellite-derived along-track and region-averaged values of SST, [Chla], and b_{bp} . The data for IB and SNS correspond to the B03 float track (note that the measurements collected prior to 5 August 2009 are used to compare with the IB region-averaged values while other measurements are used to compare with the SNS values, see Figure 1), while data for IS correspond to the B01 track float. Although the three properties exhibit large seasonal variability (the along-track SST varied

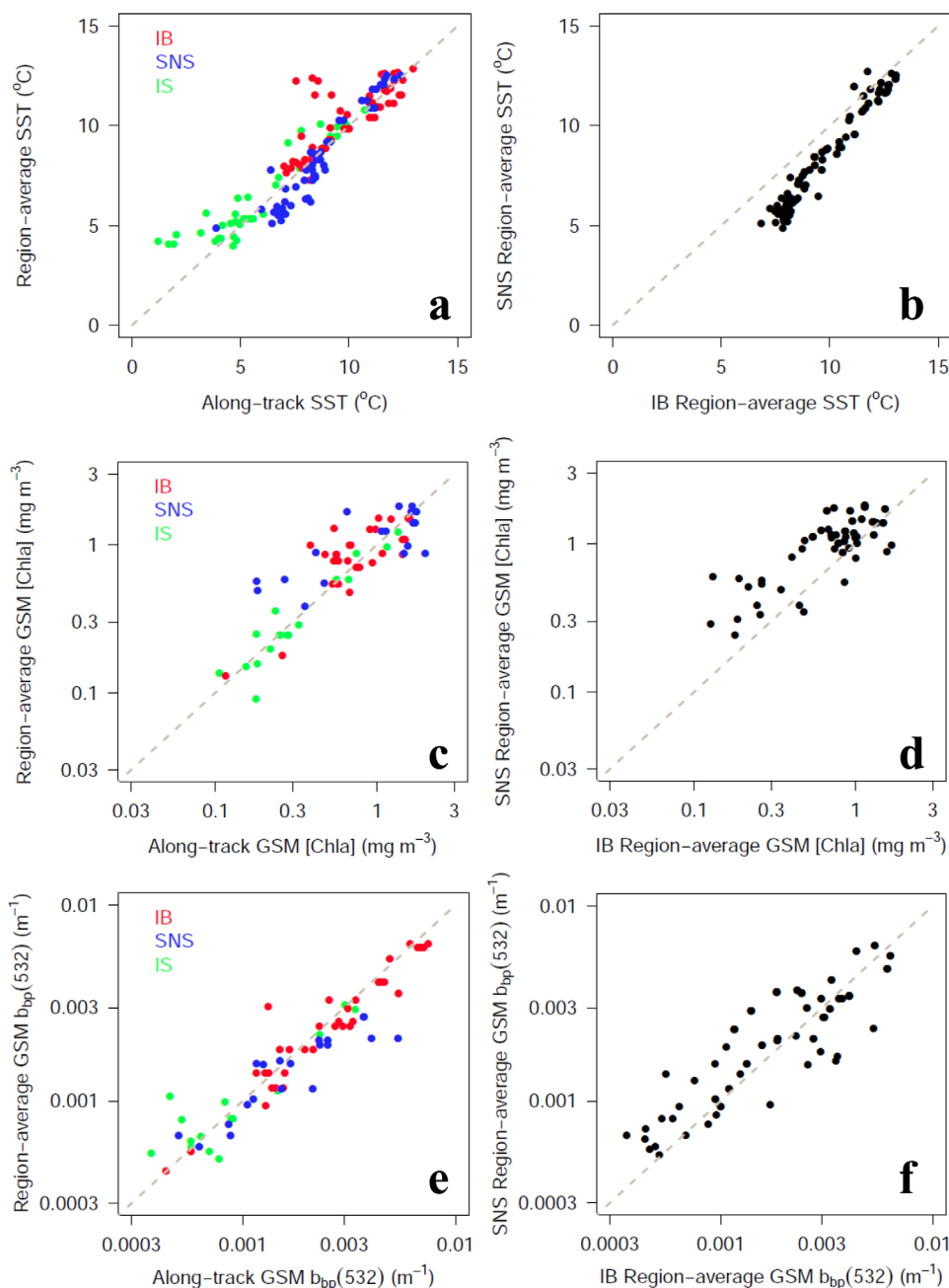


Figure 3. (a, c, and e) Scatter plots between MODIS remotely sensed along-track values (following the float trajectories) and region-averaged ones for (a) SST, (b) GSM [Chla], and (c) GSM $b_{bp}(532)$. Red dots for the Iceland Basin (IB), blue dots for the South Norwegian Sea (SNS), and green dots for the Irminger Sea (IS). (b, d, and f) Scatter plots between region-averaged values in two regions, the Iceland Basin (IB) and the South Norwegian Sea (SNS), including (b) SST, (d) GSM [Chla], and (f) GSM $b_{bp}(532)$. The gray dashed lines represent 1:1 lines.

between 1 and 13°C, and both [Chla] and b_{bp} varied within more than an order of magnitude), most data are along the 1:1 line, regardless of the region. This suggests that the floats sampled a region that was representative of their basins.

Because the B03 float drifted from the Iceland basin to the Norwegian Sea during its 2 year operation period, the region-averaged values of IB and SNS (Figures 3b, 3d, and 3f) were also compared. Unsurprisingly, the surface temperature was always lower in SNS than in IB (Figure 3b) due to a higher latitude. However, the bio-optical properties did not display remarkable differences (Figures 3d and 3f), just slightly higher [Chla] and particle backscattering values in SNS than IB.

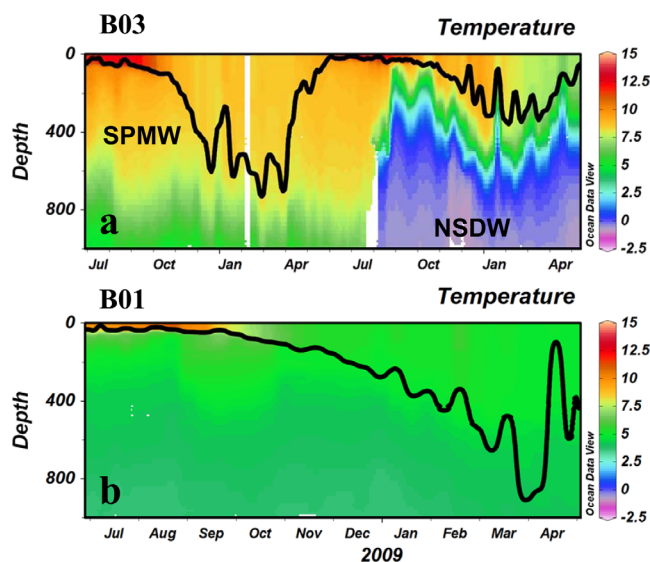


Figure 4. Time series of temperature ($^{\circ}\text{C}$) in the upper 1000 m observed by the B03 and B01 floats, respectively. The black lines represent the density-based mixed layer depth ($\text{MLD}_{d0.03}$). SPMW = Subpolar Mode Water; NSDW = Norwegian Sea Deep Water.

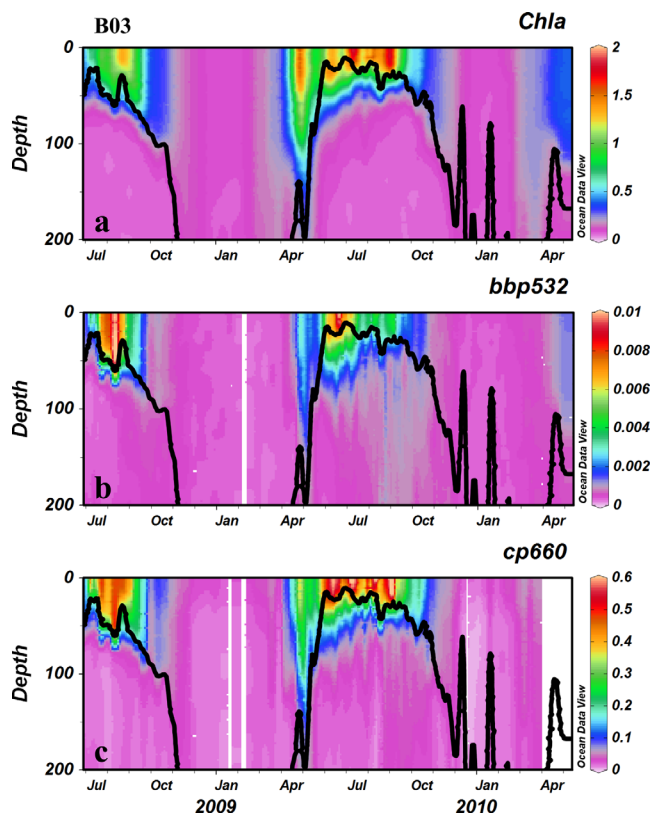


Figure 5. (a) Time series of chlorophyll-a concentration (units mg m^{-3}); (b) particle backscattering coefficient at 532 nm ($b_{bp}(532)$) (m^{-1}); and (c) particle beam attenuation coefficient at 660 nm ($c_p(660)$) (m^{-1}) in the upper 200 m, observed by the B03 float. The black lines represent the density-based mixed layer depth ($\text{MLD}_{d0.03}$).

3.2. Hydrological Background

Figure 4 showed the time series in temperature distributions from surface to 1000 m observed by two floats. As mentioned above, the B03 float remained in the Iceland Basin until July 2009, and then entered the Norwegian Sea. Correspondingly, the temperature exhibited obvious distinctions between both basins, especially below 400 m depth (Figure 4a). At the surface, the temperature varied seasonally, from $\sim 12.3^{\circ}\text{C}$ in summer, to $\sim 8.5^{\circ}\text{C}$ in winter. In the Iceland Basin, the subpolar mode water (SPMW) was located within the 100–800 m layer, and the temperature decreased gradually with depth, reaching $\sim 5^{\circ}\text{C}$ at 1000 m. In contrast, the temperature decreased very sharply with depth in the Norwegian Sea. At the surface, warm waters were brought by the Norwegian Atlantic Current (NwAC). Meanwhile, the much colder ($< 0^{\circ}\text{C}$) Norwegian Sea Deep Water (NSDW) was located at the bottom; the boundary between NwAC and NSDW was recorded at 400 m. In the Irminger Sea, the B01 float recorded different temperature structures (Figure 4b). It was much colder than the Iceland Basin, varying from $\sim 10^{\circ}\text{C}$ in summer, to $\sim 5^{\circ}\text{C}$ in winter, owing to the influence of cold East Greenland Current (EGC).

3.3. Vertical Dynamics of Bio-optical Properties

The time series of the three bio-optical properties are shown in Figures 5 (for B03) and 6 (for B01) from surface to 200 m (because their seasonal variability mainly occurred in this layer, and the maximum euphotic depth reached ~ 130 m). In general, [Chla], $b_{bp}(532)$, and $c_p(660)$ exhibited similar seasonal patterns and vertical distributions for both floats. Except for a short period in summer, the bio-optical profiles were delineated by the MLD into two layers: the “surface layer” with much higher values and very clear seasonal cycles, and the “deep layer”

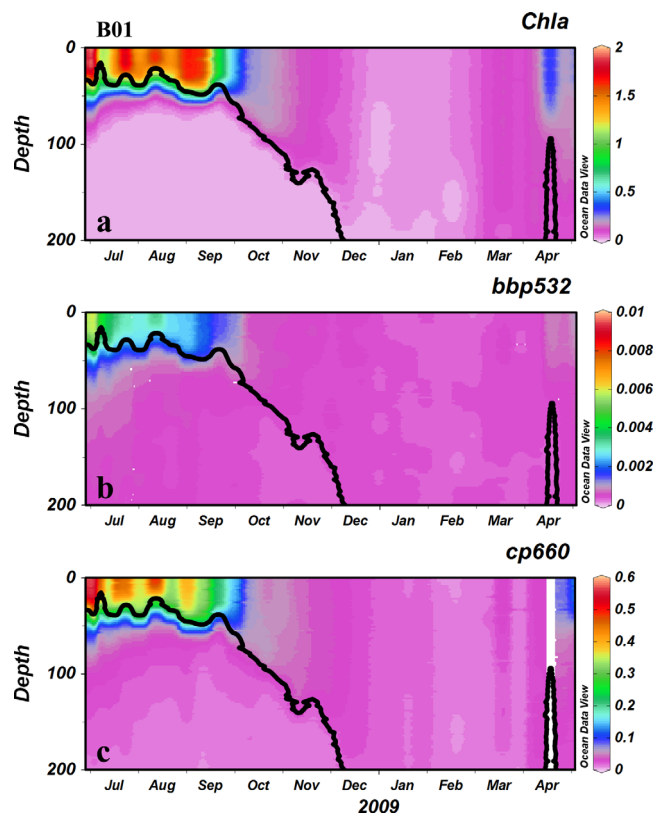


Figure 6. As for Figure 5, but for the float B01.

in July. This observation suggests that the backscattering coefficient is more sensitive to the presence of a specific phytoplankton species in summer.

3.4. Seasonal Variations of Bio-optical Properties

First, the temporal evolutions of MLD, z_{pd} , and z_{eu} are displayed in Figure 7a. MLD displayed a large seasonal variability from summer (<15 m) to winter (>300 m). Its maximum appeared in February/March, in agreement with a previous in situ observation in this region [Boss and Behrenfeld, 2010] and the climatology data set [De Boyer-Montegut et al., 2004]. Two optical properties, z_{pd} and z_{eu} , exhibited almost the same seasonal variability, shallower in summer and deeper in winter. z_{pd} varied around 10 m, and z_{eu} changed from ~ 30 to ~ 100 m. It is worth noting that z_{pd} was always shallower than the MLD, while z_{eu} was only deeper than the MLD during a short period in summer.

In order to quantitatively assess the temporal variability of bio-optical properties (presented in Figures 5 and 6), the averaged values within the penetration depth (z_{pd}) are calculated and compared with the along-track MODIS retrieved [Chla] and $b_{bp}(532)$. Due to lack of valid satellite observation during winter time, this comparison is limited to an 8 month period (from March to October).

The remotely sensed data compare relatively well with the float [Chla] and $b_{bp}(532)$, especially for the backscattering data. The correlation between the satellite-derived and float data is examined using a linear relationship (i.e., $y = A + Bx$) and a power-law relationship (i.e., $y = Ax^B$). The determination coefficients of the linear regressions (r^2) reached 0.47 and 0.78 for [Chla] and $b_{bp}(532)$, and the corresponding root mean square error (RMSE) reached 0.4 mg m^{-3} and 0.001 m^{-1} , respectively. For the power-law regression r^2 reached 0.7 (RMSE = 0.2 rel. unit) and 0.82 (RMSE = 0.15 rel. unit) for [Chla] and $b_{bp}(532)$, respectively. In addition, the scatter plots in Figure 8 indicate no systematic bias between the satellite and the float data sets.

Overall, [Chla], $b_{bp}(532)$, and $c_p(660)$ observed by floats had analogous temporal patterns, higher in spring-summer and lower in winter, exhibiting strong coupling among them (Figure 7b). All three

without any apparent biological activities, nor seasonal variations. In autumn, these properties were reduced concurrently with the mixed layer depth deepening. In winter, they all reached a temporal minimum and homogeneity from the surface to 400 m. In spring, phytoplankton began to increase significantly, and the three properties were enhanced accordingly until late summer.

Besides these first order coherent variations, some minor differences in the dynamics of these three properties still prevailed. First, the spring increase in $b_{bp}(532)$ occurs later than the increase in [Chla] and $c_p(660)$. Second, the $b_{bp}(532)$ maximum observed by the B03 float lasted over a 2 month period, in comparison with a longer period for high concentrations of [Chla] and $c_p(660)$. For example, in 2009 both [Chla] and $c_p(660)$ maintained a high level from April to September, while $b_{bp}(532)$ only peaked in June, and then began to decrease

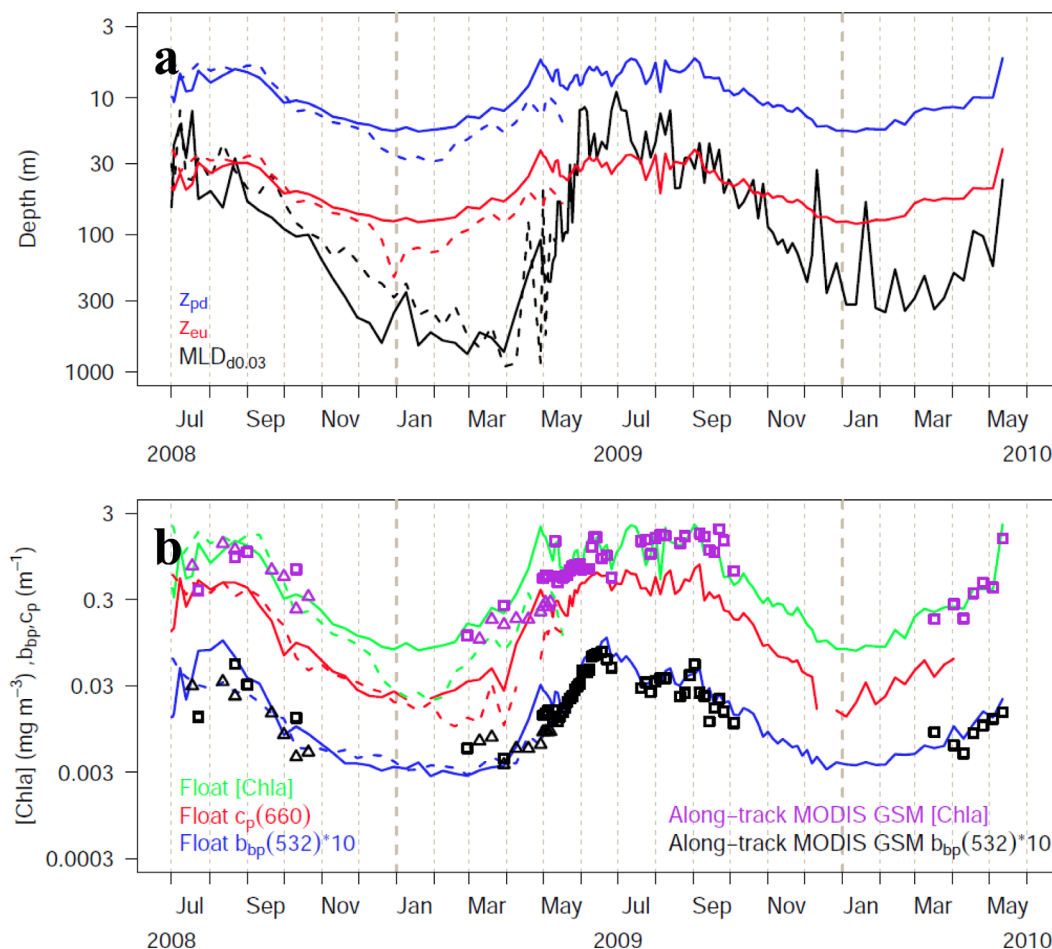


Figure 7. (a) Time series of the penetration depth (z_{pd}), the euphotic depth (z_{eu}), and the density-based mixed layer depth ($MLD_{d0.03}$). The solid and dashed lines represent the data observed by the B03 and B01 floats, respectively. (b) Time series of the averaged chlorophyll-*a* concentration ($mg\ m^{-3}$), 10 times of particle backscattering coefficient at 532 nm ($b_{bp}(532)$) (m^{-1}), and particle beam attenuation coefficient at 660 nm ($c_p(660)$) (m^{-1}) within the penetration depth (z_{pd}), as well as the along-track MODIS [Chla] and $b_{bp}(532)$ retrieved from the GSM semi-analytical model. The solid lines and square correspond to the B03 float, while the dashed lines and triangle correspond to the B01 float.

properties varied by more than an order of magnitude, [Chla] changed seasonally from 0.01 to $2\ mg\ m^{-3}$, $b_{bp}(532)$ from 0.00015 to $0.01\ m^{-1}$, and $c_p(660)$ from 0.01 to $0.7\ m^{-1}$. Note that the minima in backscattering and beam attenuation in the wintertime were very close to their respective estimated NAP values (see section 2.1). It implies that $b_{bp}(532)$ and $c_p(660)$ measurements in winter were close to or beneath their respective detection limits. Furthermore, the period during which the bio-optical variables slowly decrease lasts about 5 months (September–January), therefore much longer than the spring period characterized by a rather sharp increase of these variables, especially for c_p and [Chla]. Characterizing the spring bloom, both variables indeed increase by about one order of magnitude over the month of April.

The onset mechanism of the spring bloom is not the topic of this study. Nevertheless, the present float data provide useful time series of three bio-optical properties concurrently measured in the subpolar North Atlantic. Especially for the beam attenuation coefficient, its seasonal dynamics in this region is documented for the first time. [Chla] often varies significantly as a physiological responses to environment change (light, temperature, and nutrient availability) [Behrenfeld *et al.*, 2005] while $c_p(600)$ is considered to be significantly related to the POC concentration and phytoplankton biomass [Behrenfeld and Boss, 2006]. Therefore, the seasonal features in $c_p(600)$ and its strong coupling with [Chla], including an initiation of increase in mid-winter, and a rapid enhancement in April, will likely contribute to a further understanding of phytoplankton dynamics and the spring bloom in the North Atlantic.

Although the three properties displayed some significant coupling with each other, the seasonal variances of $b_{bp}(532)$ still presented a slight difference from [Chla] and $c_p(660)$. The backscattering signal in the

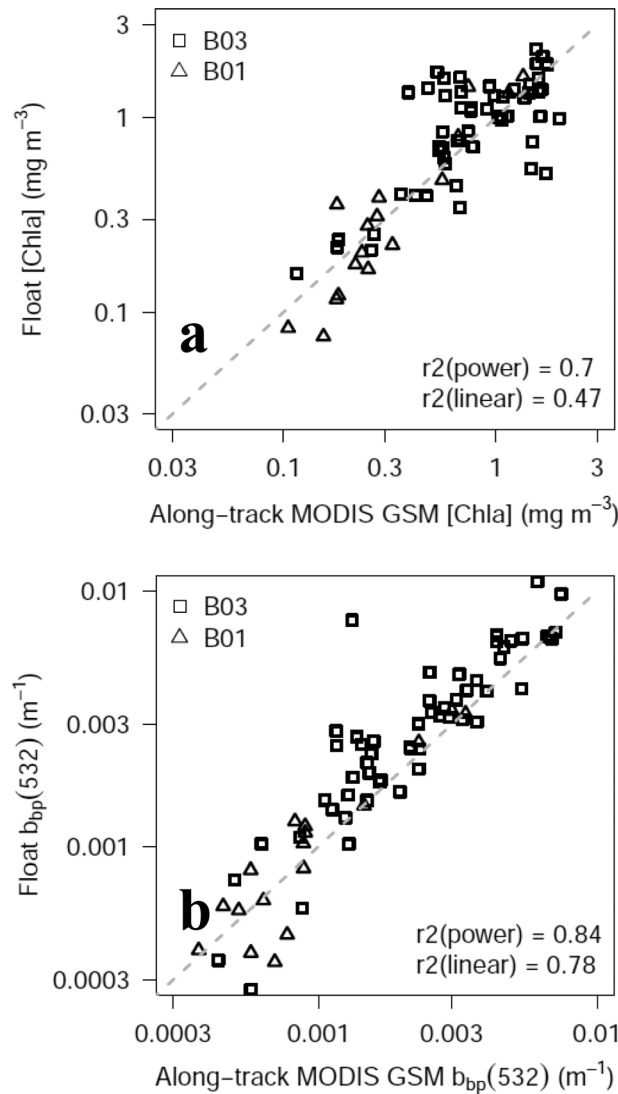


Figure 8. (a) Scatter plots between float measured [Chla] and the along-track MODIS [Chla]. The squares and triangles correspond to the B03 and B01 floats, respectively. The gray dashed lines represent 1:1 lines. (b) As for the Figure 8a, but for $b_{bp}(532)$.

corresponding formula, study areas and references as well as their abbreviations are listed in Tables 2–4.

In Figure 9a, [Chla] and $b_{bp}(532)$ displayed strong correlations, especially when $b_{bp}(532)$ was lower than 0.003 m^{-1} . The regression relationship was obtained as,

$$b_{bp}(532) = 0.003 [\text{Chla}]^{0.786} \tag{7}$$

and the determination coefficients (r^2) reached 0.81. Many large backscattering values ($>0.003 \text{ m}^{-1}$) were above the regression line, corresponding to an increase in backscattering in the IB after the spring bloom described above. Here, it is suggested that the backscattering efficiency (with respect to [Chla] or c_p) of these particles is obviously larger than for particles recorded at other periods. The [Chla] to b_{bp} relationship

Table 1. Regressed Bio-optical Relationships in This Study				
Regressed Relationship	r^2	N	Equation	Figure
$b_{bp}(532) = 0.003 [\text{Chla}]^{0.786}$	0.81	163	(7)	9a
$c_p(660) = 0.31 [\text{Chla}]^{0.981}$	0.91	156	(8)	9b
$b_{bp}(532) = 0.007 c_p(660)^{0.812}$	0.92	156	(9)	9c

obtained from the present data set is consistent with that from six previous studies, apart from one derived from Ross Sea data [Reynolds et al., 2001, Rey01b]. Both the multiplicative coefficient (0.003) and the exponent (0.786) were similar to those from the Rey01a relationship (0.004 and 0.822) obtained in the APFZ [Reynolds et al., 2001]. Specifically, with the

Iceland Basin showed a second maximum in July 2008 and June 2009, after the spring bloom. It seems to suggest the strong presence of a highly refractive material (algal species or other particles) particularly in summer after the spring bloom. Further discussion is made on this subject in section 3.6.

3.5. Interrelationships Between Bio-optical Properties

To a first order, the IOPs associated with particulate matter (e.g., b_{bp} , a_p , b_p , and c_p) depend on the concentration of the main optically significant components. In surface Case-I waters, phytoplankton are responsible for most variability in the IOPs, and their interrelationships have been studied intensively in numerous ocean regions [Loisel and Morel, 1998; Bricaud et al., 1998; Huot et al., 2008; Loisel et al., 2011; Antoine et al., 2011]. However, studies of regional bio-optical relationships, particularly focusing on seasonal cycles, still remain rare. In this section, the interrelationships between [Chla], $b_{bp}(532)$, and $c_p(660)$ are examined and compared with previous results obtained in other oceanic regions. The scatter plots of the different bio-optical properties are shown in Table 1 and Figure 9 with black lines representing best-fit regression results. Empirical relationships from previous studies are also plotted. The corre-

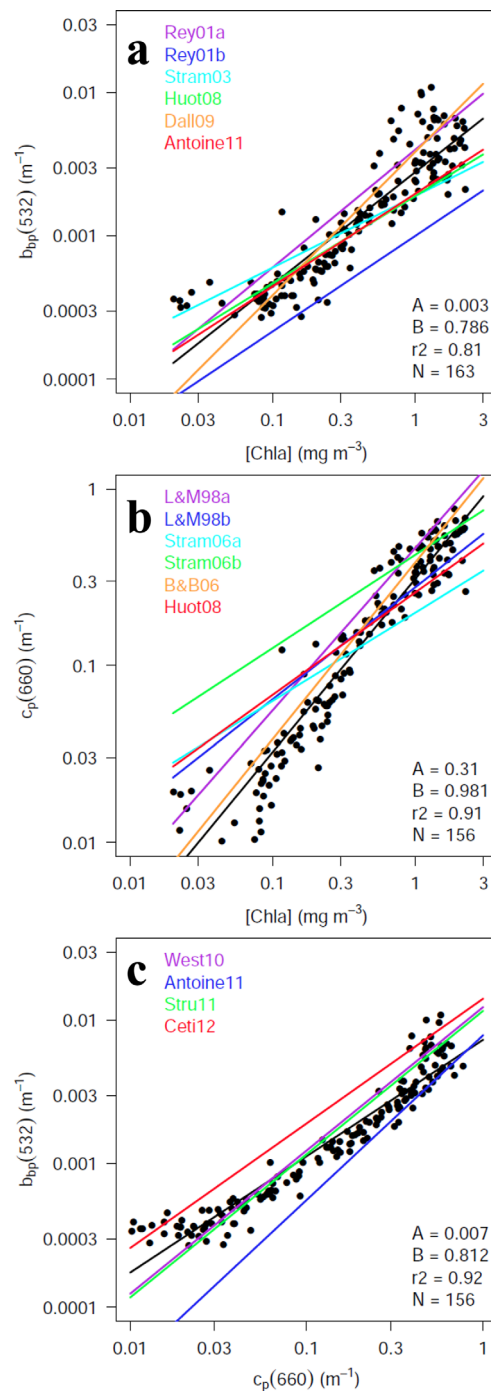


Figure 9. Scatter plots between bio-optical properties: (a) [Chla] versus $b_{bp}(532)$, (b) [Chla] versus $c_p(660)$, and (c) $c_p(660)$ versus $b_{bp}(532)$. The black lines represent the best-fit regression relationships. The colored curves were obtained previously from the studies of Reynolds *et al.* [2001] in the APFZ (Rey01a) and in the Ross Sea (Rey01b), Stramska *et al.* [2003] in the polar North Atlantic (Stram03), Huot *et al.* [2008] in the eastern South Pacific (Huot08), Dall’Omo *et al.* [2009] in the eastern Equatorial Pacific (Dall09), Antoine *et al.* [2011] in the northwestern Mediterranean Sea and Santa Barbara Channel (Antoine11), Loisel and Morel [1998] in the North Atlantic (L&M98a) and in the tropical Atlantic and Pacific, Mediterranean Sea (L&M98b), Stramska *et al.* [2006] in the polar North Atlantic in spring (Stram06a) and in summer (Stram06b), Behrenfeld and Boss [2006] in the eastern Equatorial Pacific (B&B06), Westberry *et al.* [2010] in the North Atlantic (West10), Strutton *et al.* [2011] in the Labrador Sea (Stru11), Cetinić *et al.* [2012] in the subpolar North Atlantic (Ceti12).

removal of the high backscattering values ($>0.003 \text{ m}^{-1}$), the remaining points were very consistent with the relationships of Huot *et al.* [2008, Huot08] and Antoine *et al.* [2011, Antoine11].

[Chla] exhibits a stronger correlation with $c_p(660)$ than with $b_{bp}(532)$ ($r^2 = 0.91$), therefore suggesting that chlorophyll-a is more coupled to particle attenuation than with particle backscattering (Figure 9b). The regression formula is as follows:

$$c_p(660) = 0.31 [\text{Chla}]^{0.981} \quad (8)$$

There are several studies addressing the relationship between [Chla] and $c_p(660)$ (Figure 9b and Table 4). Yet the present relationship (represented as a black line in Figure 9b) is consistent only with those from the North Atlantic [Loisel and Morel, 1998, L&M98a] and the Eastern Equatorial Pacific [Behrenfeld and Boss, 2006, B&B06]. The exponent of the present relationship (0.981) falls indeed between the exponents of the L&M98a (0.919) and B&B06 (1 for the linear relationship) relationships. Furthermore, it is noticeable that, the L&M98a relationship is based on a North Atlantic subset of a global data set [Loisel and Morel, 1998], and that the authors did discuss the particularity of the North Atlantic in the global ocean. The obvious higher exponent in this region (see the difference between L&M98a and L&M98b) was considered to be due to the presence of special particles with extremely high scattering and reflectance (likely coccolithophores or detached liths) [Loisel and Morel, 1998].

Finally, the scatter plot between particle backscattering and particle attenuation coefficients is displayed in Figure 9c. The correlation coefficient calculated here between $b_{bp}(532)$ and $c_p(660)$ is also high ($r^2 = 0.93$), suggesting the strongest coupling among the three relationships examined:

$$b_{bp}(532) = 0.007 c_p(660)^{0.812} \quad (9)$$

Similarly to Figure 9a, Figure 9c data with a high particle backscattering coefficient are observed above the regression lines, suggesting the presence of abundant particles with a higher backscattering efficiency with respect to [Chla] or c_p . Three of the

Table 2. Established Relationships Between b_{bp} and [Chla] From Previous Studies

Legend	Regression Formula	Region	Reference
Rey01a	$b_{bp}(555) = 0.004 [\text{Chla}]^{0.822}$	Antarctic Polar Front Zone (APFZ)	Reynolds et al. [2001]
Rey01b	$b_{bp}(555) = 0.001 [\text{Chla}]^{0.667}$	Ross Sea	Reynolds et al. [2001]
Stram03	$b_{bp}(555) = 0.0019 [\text{Chla}]^{0.5}$	Polar North Atlantic	Stramska et al. [2003]
Huot08	$b_{bp}(532) = 0.0019 [\text{Chla}]^{0.61}$	Eastern South Pacific	Huot et al. [2008]
Dall09 ^a	$b_{bp}(526) = 0.00386 [\text{Chla}]$	Eastern Equatorial Pacific	Dall'Olmo et al. [2009]
Antoine11	$b_{bp}(555) = 0.00197 [\text{Chla}]^{0.647}$	Northwestern Mediterranean Sea and Santa Barbara Channel	Antoine et al. [2011]

^aThe regression relationship obtained by Dall'Olmo et al. [2009] was changed here, removing the intercept of $b_{bp}(532)$ (−0.000317) that was considered as an instrumental bias.

empirical relationships from previous studies were adjusted to the wavelengths of the present study (532 nm for b_{bp} and 660 nm for c_p), assuming that particle backscattering has a spectral dependence of the λ^{-1} type. The data from the present study show a better consistency with the relationships from Westberry et al. [2010, West10] and Strutton et al. [2011, Stu11] than with those from Antoine et al. [2011, Antoine11] and Cetinić et al. [2012, Ceti12]. The regression exponent (0.812) derived from the present data set is very close to that of Ceti12 (0.871) which was obtained in the same region (the Iceland Basin).

3.6. Temporal Variability of Ratios

Although [Chla], b_{bp} , and c_p appear to be well coupled, some slight seasonal and vertical discrepancies between them are still noticed, for example, the particular enhancement of b_{bp} in summer. In this section, the time series of their ratios ($b_{bp}(532)/c_p(660)$ and $[\text{Chla}]/c_p(660)$) are examined to investigate the possible influence of particle size distribution and phytoplankton photoacclimation.

At 660 nm, particulate and dissolved absorptions are negligible so that $c_p(660)$ approximately equals scattering coefficient, $b_p(660)$ [Loisel et al., 2007]. As a consequence, the ratio of $b_{bp}(532)/c_p(660)$ can be analyzed as the $b_{bp}(532)/b_p(660)$ ratio. This ratio can be further expressed as the product of two terms, $b_{bp}(532)/b_{bp}(660)$ and $b_{bp}(660)/b_p(660)$. The former is proportional to the backscattering spectral exponent [Loisel et al., 2006], and the latter is known as the backscattering ratio [Ulloa et al., 1994; Twardowski et al., 2001; Loisel et al., 2007]. To first order, the particle backscattering spectral exponent increases as the proportion of small particles increases and reciprocally [Kostadinov et al., 2009]. The b_{bp}/b_p ratio responds significantly to the composition of particulate matter, being large when inorganic particles dominate [Twardowski et al., 2001; Loisel et al., 2007]. As a result, the ratio $b_{bp}(532)/c_p(660)$ could be considered as a proxy of particle size and composition, increasing when small or inorganic particles become relatively more abundant than large or organic particles. As shown in Figure 10a, this ratio displayed a remarkable summer peak (July–August 2008, June 2009) in the Iceland Basin, suggesting the presence of small phytoplankton or highly refractive inorganic matter (e.g., nanoflagellates or coccolithophores) after the spring bloom, which was most likely associated with diatoms (generally microphytoplankton). Obviously, no ancillary measurements are available to support the present hypothesis. A certain number of former studies nevertheless help in supporting it. Based on in situ observations in the Gulf of Maine, Balch et al. [1991] proposed that the particle backscattering coefficient was more sensitive to the abundance of coccolithophores than the beam attenuation coefficient. Besides, Fernandez et al. [1993] reported a large-scale coccolithophore bloom characterized by high particulate inorganic carbon (PIC) in the Iceland Basin in late June 1991. Here, the along-track remotely sensed PIC data indicated that the suspended calcium carbonate (CaCO_3) was remarkably enhanced in the summer of 2008 and 2009, with its maximum corresponding to the summer peak of b_{bp} and b_{bp}/c_p (Figure 10a). We thus suggest that a coccolithophore bloom was responsible for the increase in the particle backscattering coefficient in the summer of 2008 and 2009 and thus for higher particle backscattering for a given [Chla] or $c_p(660)$.

Theoretically, the variability of c_p is dominated by the concentration of particles, and thus c_p has been used to quantitatively estimate POC over diverse ocean environments [Gardner et al., 1985; Claustre et al., 1999; Oubelkheir et al., 2005; Behrenfeld and Boss, 2006; Gardner et al., 2006], including the subpolar North Atlantic [Cetinić et al., 2012]. On the other hand, the chlorophyll-a concentration is often affected by the so-called “photoacclimation” process (i.e., an intracellular change in [Chla] which results from a physiological adaptation of phytoplankton cells to the ambient light conditions), although it has been used as a proxy of

Table 3. Established Relationships Between c_p and [Chla] From Previous Studies

Legend	Regression Formula	Region	Reference
L&M98a	$c_p(660) = 0.464 [\text{Chla}]^{0.919}$	North Atlantic	<i>Loisel and Morel</i> [1998]
L&M98b	$c_p(660) = 0.278 [\text{Chla}]^{0.634}$	Tropical Atlantic and Pacific, Mediterranean Sea	<i>Loisel and Morel</i> [1998]
Stram06a	$c_p(660) = 0.1995 [\text{Chla}]^{0.4995}$	Polar North Atlantic (spring)	<i>Stramska et al.</i> [2006]
Stram06b	$c_p(660) = 0.4244 [\text{Chla}]^{0.5282}$	Polar North Atlantic (summer)	<i>Stramska et al.</i> [2006]
B&B06 ^a	$[\text{Chla}] = 2.6c_p(660)$	Eastern Equatorial Pacific	<i>Behrenfeld and Boss</i> [2006]
Huot08	$b_p(650) = 0.26 [\text{Chla}]^{0.58}$	Eastern South Pacific	<i>Huot et al.</i> [2008]

^aThe regression relationship obtained by *Behrenfeld and Boss* [2006] was changed here, removing the intercept of [Chla] (0.014) that was considered as an instrumental bias.

phytoplankton biomass for about half a century [*Lorenzen, 1966; Cullen, 1982, Behrenfeld et al., 2005*]. Thus, the ratio of [Chla] to $c_p(660)$ could be considered as a physiological parameter, in proportion to the chlorophyll-a content for per unit phytoplankton carbon (i.e., [Chla]:C). This parameter has previously been well documented in situ and in cultures [*Geider, 1987, Geider et al., 1998; Behrenfeld and Boss, 2003, 2006*], and it is here expected to depend on the light intensity at the first order. Nevertheless, it should be noted that if the [Chla]: c_p ratio should not be exclusively controlled by photoacclimation, then the relative contributions of phytoplankton and nonalgal materials would also influence this ratio [*Sathyendranath et al., 2009*].

The time series of [Chla]/ $c_p(660)$ and the concurrent growth irradiance (I_g) values derived from the float [Chla] profiles, satellite PAR and in situ determined MLD (see section 2.3), are depicted in Figure 10b. Apart from some abnormal values of B01 during wintertime, the ratio [Chla]/ $c_p(660)$ displays a clear seasonal cycle, higher in winter and lower in summer. It thus appears to be negatively correlated to the light level. (Note that I_g was plotted reversely in Figure 10b.) The scatter plot between both quantities (Figure 10c) follows the photoacclimation model proposed by *Behrenfeld et al.* [2002, 2005]. Their relationship can be expressed as:

$$[\text{Chla}]/c_p(660) = 1.859 + 1.985 \exp(-3I_g) \quad (10)$$

with $r^2 = 0.445$. It also can be written as

$$[\text{Chla}]/c_p(660) = 1.859 + (3.844 - 1.859) \exp(-3I_g) \quad (10')$$

Here, 1.859 and 3.844 represent the possible minimum and maximum ratio of [Chla]/ $c_p(660)$, respectively. This means the seasonal variability of photoacclimation can possibly cause a twofold change in [Chla]/ $c_p(660)$. It is noticeable that the maximum ratio (3.844) has a much larger uncertainty than the minimum one, as the former was obtained in wintertime when both [Chla] and $c_p(660)$, respectively, reached their lowest values and were highly sensitive to the correction method (presented in section 2.1). For further comparison with the results of *Behrenfeld et al.* [2005] based on satellite data, the regression slope parameter between $c_p(660)$ and POC obtained by *Cetinić et al.* [2012] in the Iceland Basin (391 mg m^{-2}) is used, as well as an assumption of a constant proportion of phytoplankton carbon (30% of POC) [*Behrenfeld et al., 2005*]. Hence, the [Chla]/ $c_p(660)$ ratio can be converted to [Chla]:C, and the minimum and maximum [Chla]:C (denoted as Chl:C_{\min} and Chl:C_{\max}) are 0.0158 and 0.0327, respectively. The corresponding parameters estimated by *Behrenfeld et al.* [2005] were 0.0133 and 0.016, in the eutrophic North Atlantic that includes the subpolar region (see their Table 1 and Figure 2a). The present values are larger than those derived from the satellite data, especially for the Chl:C_{\max} . As mentioned above, the much higher Chl:C_{\max} was most likely

Table 4. Established Relationships Between b_{bp} and c_p From Previous Studies

Legend	Regression Formula	Region	Reference
West10 ^a	$b_{bp}/c_p = 0.01$	North Atlantic	<i>Westberry et al.</i> [2010]
Antoine11	$b_{bp}(555) = 0.0079 c_p(660)^{1.149}$	Northwestern Mediterranean Sea and Santa Barbara Channel	<i>Antoine et al.</i> [2011]
Stru11 ^a	$c_p(660) = 75.57 b_{bp}(470)$	Labrador Sea	<i>Strutton et al.</i> [2011]
Ceti12 ^a	$b_{bp}(700) = 0.0108c_p(653)^{0.871} (bbp \sim \lambda^{-1})$	Subpolar North Atlantic	<i>Cetinić et al.</i> [2012]

^aThe regression relationships were converted to b_{bp} at 532 nm when plotting in Figure 9c, assuming a spectral dependence of λ^{-1} for backscattering.

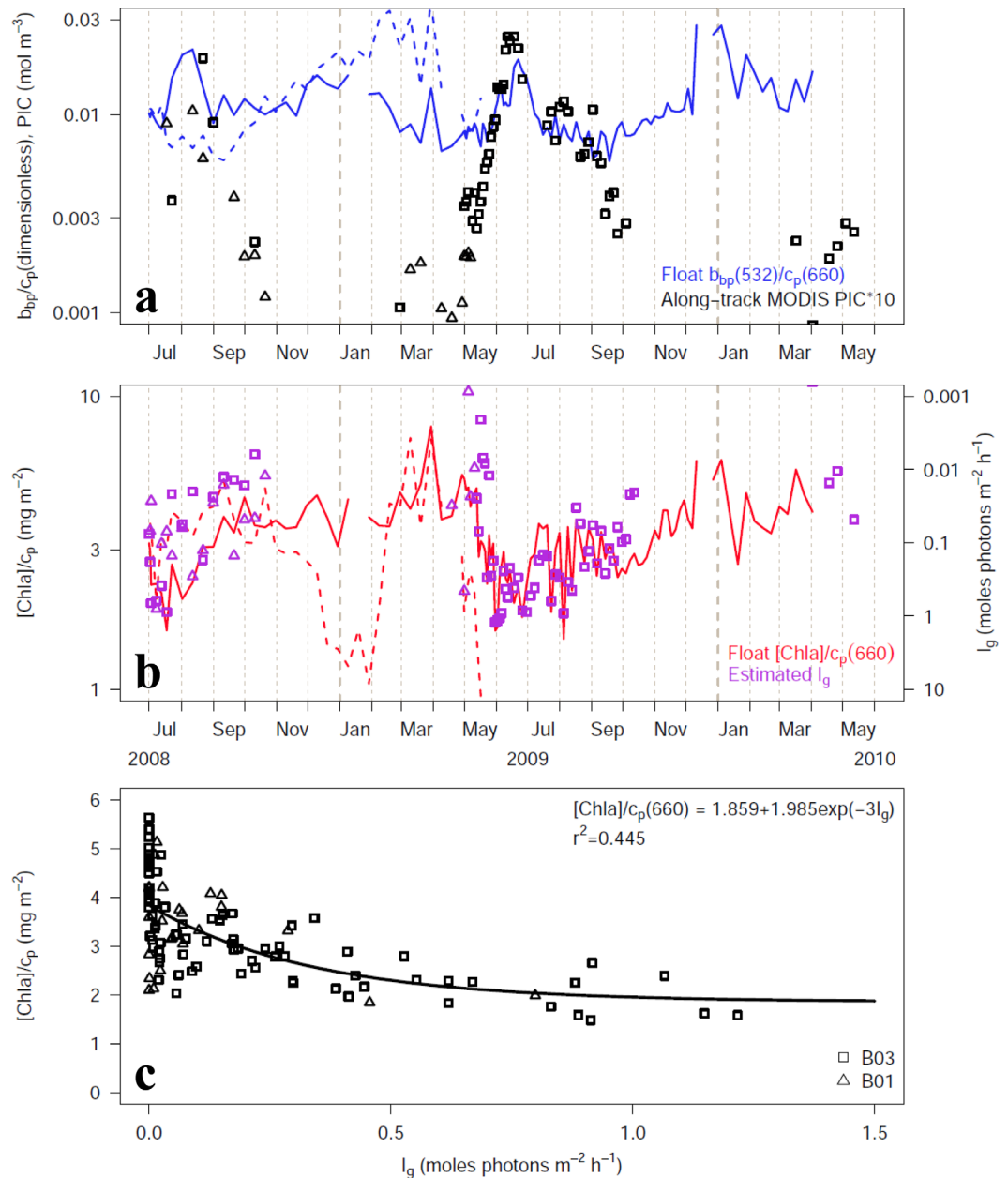


Figure 10. (a) Time series of float-measured $b_{bp}(532)/c_p(660)$ (dimensionless) and MODIS remotely sensed particulate inorganic carbon (PIC) concentration (mol m^{-3}). Note that PIC has been multiplied by ten, in order to share the left axis with b_{bp}/c_p . (b) Time series of float-measured $[\text{Chla}]/c_p(660)$ (mg m^{-2}) and estimated growth irradiance (I_g) (moles photons $\text{m}^{-2} \text{h}^{-1}$). Note that the right axes for I_g are reversed. (c) Scatter plot between I_g and $[\text{Chla}]/c_p(660)$; the black line represents the best-fit regression line.

due to the measurement uncertainty. However, the higher $\text{Chl:C}_{\text{min}}$ was probably more realistic, likely because it is from a northernmost area than the one studied by *Behrenfeld et al.* [2005] and hence less subjected to nutrient stress, owing to stronger vertical mixing.

4. Final Remarks and Conclusions

Overall, the seasonal and vertical patterns of three bio-optical properties ($[\text{Chla}]$, $b_{bp}(532)$, and $c_p(660)$) in the subpolar North Atlantic were mainly characterized by a deep mixing in autumn-winter and a phytoplankton bloom in spring-summer. The three properties were found to be largely coupled within the mixed layer, indicating that, at first order, phytoplankton and co-varying particles were the main contributors to

these properties; this is a typical example of the so-called case I waters [Morel, 1988]. The particle backscattering coefficient obviously appears more dependent upon inorganic particles rather than organic ones, suggesting that the increase in $b_{bp}(532)$ and $b_{bp}(532)/c_p(660)$ in late summer is likely associated to a coccolithophore bloom. Furthermore, and considering $b_{bp}(532)$ dynamics, the Iceland Basin and the Irminger Sea, appear to have differing particle compositions.

The present study has shown that relationships between key bio-optical variables acquired by floats can accurately be established and further compared to other global or regional relationships. This, in some way, constitutes an important validation step in the acquisition of time series of bio-optical properties in a totally autonomous way. With the development of a global Bio-Argo float network, the database of bio-optical properties will drastically increase in a near-future. As a consequence, a refinement of the established relationships can be expected, with regional and/or temporal nuances in these relationships being likely better addressed and understood. In turn these refinements could help in identifying the oceanic regions and/or period of interest where classical ship-based operations would allow for a full understanding of the main biogeochemical and bio-optical processes at play.

Acknowledgments

This paper represents a contribution to the remOcean (REMotely sensed biogeochemical cycles in the OCEAN, GA 246777) project funded by the European Research Council, to the PABO (Plateformes Autonomes et Biogéochimie Océanique) project, funded by Agence Nationale de la Recherche, to the OSS2015 (Ocean Strategic Services beyond 2015) EU-FP7 project, to the National Natural Science Foundation of China (41206028, 41023007, 41276186), to the National Basic Research Program of China under contract no. 2011CB403501, to the Public Science and Technology Research Funds Projects of Ocean (201005030), and to the MEL Visiting Fellowship Program (MELRS1220). We are particularly grateful to Emmanuel Boss and to an anonymous reviewer for useful comments and suggestions they made on the first version of the present paper. Joséphine Ras is acknowledged for careful polishing of the English. The float data used in this study can be found at: <http://www.oao.obs-vlfr.fr/provbio/summary.html>.

References

- Antoine, D., D. A. Siegel, T. Kostadinov, S. Maritorena, N. B. Nelson, B. Gentili, V. Vellucci, and N. Guillocheau (2011), Variability in optical particle backscattering in three contrasting bio-optical oceanic regimes, *Limnol. Oceanogr. Methods*, *56*, 955–973.
- Balch, W. M., P. M. Holligan, S. G. Ackleson, and K. J. Voss (1991), Biological and optical properties of mesoscale coccolithophore blooms in the Gulf of Maine, *Limnol. Oceanogr.*, *36*, 629–643.
- Balch, W. M., D. T. Drapeau, J. J. Fritz, B. C. Bowler, and J. Nolan (2001), Optical backscattering in the Arabian Sea: Continuous underway measurements of particulate inorganic and organic carbon, *Deep Sea Res., Part I*, *48*, 2423–2452.
- Balch, W. M., H. R. Gordon, B. C. Bowler, D. T. Drapeau, and E. S. Booth (2005), Calcium carbonate measurements in the surface global ocean based on Moderate-Resolution Imaging Spectroradiometer data, *J. Geophys. Res.*, *110*, C07001, doi:10.1029/2004JC002560.
- Behrenfeld, M. J. (2010), Abandoning Sverdrup's Critical Depth Hypothesis on phytoplankton blooms, *Ecology*, *91*(4), 977–989.
- Behrenfeld, M. J., and E. Boss (2003), The beam attenuation to chlorophyll ratio: An optical index of phytoplankton physiology in the surface ocean?, *Deep Sea Res., Part I*, *50*, 1537–1549.
- Behrenfeld, M. J., and E. Boss (2006), Beam attenuation and chlorophyll concentration as alternative optical indices of phytoplankton biomass, *J. Mar. Res.*, *64*, 431–451, doi:10.1357/002224006778189563.
- Behrenfeld, M. J., and E. S. Boss (2014), Resurrecting the ecological underpinnings of ocean plankton blooms, *Ann. Rev. Mar. Sci.*, *6*, 167–194.
- Behrenfeld, M. J., E. Maranon, D. A. Siegel, and S. B. Hooker (2002), A photoacclimation and nutrient based model of light-saturated photosynthesis for quantifying oceanic primary production, *Mar. Ecol. Prog. Ser.*, *228*, 103–117.
- Behrenfeld, M. J., E. Boss, D. A. Siegel, and D. M. Shea (2005), Carbon-based ocean productivity and phytoplankton physiology from space, *Global Biogeochem. Cycles*, *19*, GB1006, doi:10.1029/2004GB002299.
- Behrenfeld, M. J., S. C. Doney, I. Lima, E. S. Boss, and D. A. Siegel (2013), Reply to a comment by Stephen M. Chiswell on: "Annual cycles of ecological disturbance and recovery underlying the subarctic Atlantic spring plankton bloom" by M. J. Behrenfeld et al. (2013), *Global Biogeochem. Cycles*, *27*, 1294–1296, doi:10.1002/2013GB004720.
- Bishop, J. K. B. (1986), The correction and suspended particulate matter calibration of the Sea Tech transmissometer data, *Deep Sea Res., Part A*, *33*, 121–134.
- Bishop, J. K. B., and T. J. Wood (2009), Year-round observations of carbon biomass and flux variability in the Southern Ocean, *Global Biogeochem. Cycles*, *23*, GB2019, doi:10.1029/2008GB003206.
- Bishop, J. K. B., S. E. Calvert, and M. Y.-S. Soon (1999), Spatial and temporal variability of POC in the Northeast Subarctic Pacific, *Deep Sea Res., Part II*, *46*, 2699–2733.
- Boss, E., and W. S. Pegau (2001), The relationship of light scattering at an angle in the backward direction to the backscattering coefficient, *Appl. Opt.*, *40*, 5503–5507.
- Boss, E., and M. J. Behrenfeld (2010), In-situ evaluation of the initiation of the North Atlantic phytoplankton bloom, *Geophys. Res. Lett.*, *37*, L18603, doi:10.1029/2010GL044174.
- Boss, E., D. Swift, L. Taylor, P. Brickley, R. Zaneveld, S. Riser, M. J. Perry, and P. G. Strutton (2008), Observations of pigment and particle distributions in the western North Atlantic from an autonomous float and ocean color satellite, *Limnol. Oceanogr. Methods*, *53*, 2112–2122.
- Bricaud, A., A. Morel, M. Babin, K. Allali, and H. Claustre (1998), Variations of light absorption by suspended particles with chlorophyll a concentration in oceanic (case 1) waters: Analysis and implications for bio-optical models, *J. Geophys. Res.*, *103*, 31,033–31,044.
- Cetinić, I., M. J. Perry, N. T. Briggs, E. Kallin, E. A. D'Asaro, and C. M. Lee (2012), Particulate organic carbon and inherent optical properties during 2008 North Atlantic Bloom Experiment, *J. Geophys. Res.*, *117*, C06028, doi:10.1029/2011JC007711.
- Claustre, H., A. Morel, M. Babin, C. Cailliau, D. Marie, J. C. Marty, D. Tailliez, and D. Vaulot (1999), Variability in particle attenuation and chlorophyll fluorescence in the tropical Pacific: Scales, patterns, and biogeochemical implications, *J. Geophys. Res.*, *104*, 3401–3422.
- Claustre, H., A. Sciandra, and D. Vaulot (2008), Introduction to the special section bio-optical and biogeochemical conditions in the South East Pacific in late 2004: the BIOSOPE program, *Biogeosciences*, *5*, 679–691.
- Claustre, H., et al. (2010), Bio-optical profiling floats as new observational tools for biogeochemical and ecosystem studies, in *Proceedings of the "OceanObs'09: Sustained Ocean Observations and Information for Society" Conference, Venice, Italy, 21–25 Sep.*, vol. 2, edited by J. Hall, D. E. Harrison, and D. Stammer, *ESA Publ. WPP-306*, doi:10.5270/OceanObs09.cwp.17.
- Cullen, J. J. (1982), The deep chlorophyll maximum: Comparing vertical profiles of chlorophyll a, *Can. J. Fish. Aquat. Sci.*, *9*, 791–803.
- Dall'Olmo, G., T. K. Westberry, M. J. Behrenfeld, E. Boss, and W. H. Slade (2009), Significant contribution of large particles to optical backscattering in the open ocean, *Biogeosciences*, *6*, 947–967.
- De Boyer Montégut, C., G. Madec, A. S. Fischer, A. Lazar, and D. Iudicone (2004), Mixed layer depth over the global ocean: An examination of profile data and a profile-based climatology, *J. Geophys. Res.*, *109*, C12003, doi:10.1029/2004JC002378.

- Fernandez, E., P. Boyd, P. M. Holligan, and D. S. Harbour (1993), Production of organic and inorganic carbon within a large-scale coccolithophore bloom in the northeast Atlantic Ocean, *Mar. Ecol. Prog. Ser.*, *97*, 271–285.
- Frouin, R., and B. Chertock (1992), A technique for global monitoring of net solar irradiance at the ocean surface. Part I: Model, *J. Appl. Meteorol.*, *31*, 1056–1066.
- Gardner W. D., P. E. Biscaye, J. R. V. Zaneveld, and M. J. Richardson (1985), Calibration and comparison of the LDGO nephelometer and the OSU transmissometer on the Nova Scotian Rise, *Mar. Geol.*, *66*, 323–344.
- Gardner, W. D., A. Mishonov, and M. J. Richardson (2006), Global POC concentrations from in-situ and satellite data, *Deep Sea Res., Part II*, *53*, 718–740.
- Geider, R. J. (1987), Light and temperature dependence of the carbon to chlorophyll ratio in microalgae and cyanobacteria: Implications for physiology and growth of phytoplankton, *New Phytol.*, *106*, 1–34.
- Geider, R. J., H. L. MacIntyre, and T. M. Kana (1998), A dynamic regulatory model of phytoplankton acclimation to light, nutrients, and temperature, *Limnol. Oceanogr.*, *43*, 679–694.
- Gordon, H. R., and A. Morel (1983), *Remote Assessment of Ocean Color for Interpretation of Satellite Visible Imagery: A Review*, 114 pp., Springer, N. Y.
- Holm-Hansen, O., A. F. Amos, and C. D. Hewes (2000), Reliability of estimating chlorophyll-a concentrations in Antarctic waters by measurement of in situ chlorophyll-a fluorescence, *Mar. Ecol. Prog. Ser.*, *196*, 103–110.
- Huot, Y., A. Morel, M. S. Twardowski, D. Stramski, and R. A. Reynolds (2008), Particle optical backscattering along a chlorophyll gradient in the upper layer of the eastern South Pacific Ocean, *Biogeosciences*, *5*, 495–507.
- International Ocean-Color Coordinating Group (IOCCG) (2011), Bio-optical sensors on Argo floats, vol. 11, edited by H. Claustre, Dartmouth, Canada.
- Kostadinov, T. S., D. A. Siegel, and S. Maritorena (2009), Retrieval of the particle size distribution from satellite ocean color observations, *J. Geophys. Res.*, *114*, C09015, doi:10.1029/2009JC005303.
- Loisel, H., and A. Morel (1998), Light scattering and chlorophyll concentration in case 1 waters: A reexamination, *Limnol. Oceanogr.*, *43*, 847–858.
- Loisel, H., J.-M. Nicolas, A. Sciandra, D. Stramski, and A. Poteau (2006), Spectral dependency of optical backscattering by marine particles from satellite remote sensing of the global ocean, *J. Geophys. Res.*, *111*, C09024, doi:10.1029/2005JC003367.
- Loisel, H., X. Meriaux, J. F. Berthon, and A. Poteau (2007), Investigation of the optical backscattering to scattering ratio of marine particles in relation to their biogeochemical composition in the eastern English Channel and southern North Sea, *Limnol. Oceanogr. Methods*, *52*, 739–752.
- Loisel, H., et al. (2011), Characterization of the bio-optical anomaly and diurnal variability of particulate matter, as seen from scattering and backscattering coefficients, in ultra-oligotrophic eddies of the Mediterranean Sea, *Biogeosciences*, *8*, 3295–3317.
- Lorenzen, C. (1966), A method for the continuous measurement of in vivo chlorophyll concentration, *Deep Sea Res. Oceanogr. Abstr.*, *13*, 223–227.
- Maritorena, S., D. A. Siegel, and A. R. Peterson (2002), Optimization of a semianalytical ocean color model for global-scale applications, *Appl. Opt.*, *41*, 2705–2714.
- Mignot, A., H. Claustre, J. Uitz, A. Poteau, F. D'Ortenzio, and X. Xing (2014), Understanding the seasonal dynamics of phytoplankton biomass and the deep chlorophyll maximum in oligotrophic environments: A Bio-Argo float investigation, *Global Biogeochem. Cycles*, *28*, 856–876, doi:10.1002/2013GB004781.
- Morel, A. (1988), Optical modeling of the upper ocean in relation to its biogenous matter content (Case I waters), *J. Geophys. Res.*, *93*, 10,749–10,768.
- Morel, A., and Y. H. Ahn (1991), Optics of heterotrophic nanoflagellates and ciliates: A tentative assessment of their scattering role in oceanic waters compared to those of bacterial and algal cells, *J. Mar. Res.*, *49*, 177–202.
- Morel, A., and A. Bricaud (1986), Inherent properties of algal cells including picoplankton: Theoretical and experimental results, *Can. Bull. Fish. Aquat. Sci.*, *214*, 521–559.
- Morel, A., and S. Maritorena (2001), Bio-optical properties of oceanic waters: A reappraisal, *J. Geophys. Res.*, *106*, 7163–7180.
- Morel, A., Y. Huot, B. Gentili, P. J. Werdell, S. B. Hooker, and B. A. Franz (2007), Examining the consistency of products derived from various ocean color sensors in open ocean (case 1) waters in the perspective of a multi-sensor approach, *Remote Sens. Environ.*, *111*, 69–88.
- Oubelkheir, K. J., H. Claustre, A. Sciandra, and M. Babin (2005), Bio-optical and biogeochemical properties of different trophic regimes in oceanic waters, *Limnol. Oceanogr. Methods*, *50*, 1795–1809.
- O'Reilly, J. E., S. Maritorena, B. G. Mitchell, D. A. Siegel, K. L. Carder, S. A. Garver, M. Kahru, and C. McClain (1998), Ocean color chlorophyll algorithms for SeaWiFS, *J. Geophys. Res.*, *103*, 24,937–24,953.
- Reynolds, R. A., D. Stramski, and B. G. Mitchell (2001), A chlorophyll-dependent semianalytical model derived from field measurements of absorption and backscattering coefficients within the Southern Ocean, *J. Geophys. Res.*, *106*, 7125–7138.
- Sathyendranath, S., V. Stuart, A. Nair, K. Oka, T. Nakane, H. Bouman, M. Forget, H. Maass, and T. Platt (2009), Carbon-to-chlorophyll ratio and growth rate of phytoplankton in the sea, *Mar. Ecol. Prog. Ser.*, *383*, 73–84.
- Smith, R. C., and K. S. Baker (1978), The bio-optical state of ocean waters and remote sensing, *Limnol. Oceanogr.*, *23*, 247–259.
- Stramska, M., D. Stramski, R. Hapter, S. Kaczmarek, and J. Stoń (2003), Bio-optical relationships and ocean color algorithms for the north polar region of the Atlantic, *J. Geophys. Res.*, *108*(C5), 3143, doi:10.1029/2001JC001195.
- Stramska, M., D. Stramski, S. Kaczmarek, D. B. Allison, and J. Schwarz (2006), Seasonal and regional differentiation of bio-optical properties within the north polar Atlantic, *J. Geophys. Res.*, *111*, C08003, doi:10.1029/2005JC003293.
- Stramski, D., and D. A. Kiefer (1991), Light scattering by microorganisms in the open ocean, *Prog. Oceanogr.*, *28*, 343–383.
- Stramski, D., R. A. Reynolds, M. Kahru, and B. G. Mitchell (1999), Estimation of particulate organic carbon in the ocean from satellite remote sensing, *Science*, *285*, 239–242.
- Strutton, P. G., T. R. Martz, M. D. DeGrandpre, W. R. McGillis, W. M. Drennan, and E. Boss (2011), Bio-optical observations of the 2004 Labrador Sea phytoplankton bloom, *J. Geophys. Res.*, *116*, C11037, doi:10.1029/2010JC006872.
- Taylor, J. R., and R. Ferrari (2011), Shutdown of turbulent convection as a new criterion for the onset of spring phytoplankton blooms, *Limnol. Oceanogr. Methods*, *56*, 2293–2307.
- Twardowski, M. S., E. Boss, J. B. Macdonald, W. S. Pegau, A. H. Barnard, and J. R. V. Zaneveld (2001), A model for estimating bulk refractive index from the optical backscattering ratio and the implications for understanding particle composition in case I and case II waters, *J. Geophys. Res.*, *106*, 14,129–14,142.
- Ulloa, O., S. Sathyendranath, and T. Platt (1994), Effect of the particle-size distribution on the backscattering ratio in seawater, *Appl. Opt.*, *30*, 7070–7077.

- Westberry, T. K., G. Dall'Olmo, E. Boss, M. J. Behrenfeld, and T. Moutin (2010), Coherence of particulate beam attenuation and backscattering coefficients in diverse open ocean environments, *Opt. Express*, *18*, 15,419–15,425.
- Xing, X., A. Morel, H. Claustre, D. Antoine, F. D'Ortenzio, A. Poteau, and A. Mignot (2011), Combined processing and mutual interpretation of radiometry and fluorimetry from autonomous profiling bio-Argo floats: Chlorophyll a retrieval, *J. Geophys. Res.*, *116*, C06020, doi: 10.1029/2010JC006899.
- Xing, X., H. Claustre, S. Blain, F. D'Ortenzio, D. Antoine, J. Ras, and C. Guinet (2012), Quenching correction for in vivo chlorophyll fluorescence acquired by autonomous platforms: A case study with instrumented elephant seals in the Kerguelen region (Southern Ocean), *Limnol. Oceanogr. Methods*, *10*, 483–495.
- Xing, X., H. Claustre, H. Wang, A. Poteau, and F. D'Ortenzio (2014), Seasonal dynamics in colored dissolved organic matter in the Mediterranean Sea: Patterns and drivers, *Deep Sea Res., Part 1*, *83*, 93–101.